1-1-2015

N-doped pierced graphene microparticles as a highly active electrocatalyst for Li-air batteries

Tao Yuan
Shanghai Jiao Tong University

Weimin Zhang
Shanghai Jiao Tong University, weimin@uow.edu.au

Wen-Ting Li
Shanghai Jiao Tong University

Chuantao Song
Shanghai Jiao Tong University

Yu-Shi He
Shanghai Jiao Tong University

See next page for additional authors

N-doped pierced graphene microparticles as a highly active electrocatalyst for Li-air batteries

Abstract

In this work we report a novel scalable strategy to prepare a lithium-air battery electrode from 3D N-doped pierced graphene microparticles (N-PGM) with highly active performance. This approach has combined the merits of spray drying technology and the hard template method. The pierced structured graphene microparticles were characterized physically and electrochemically. An x-ray photoelectron spectrometer and Raman spectra have revealed that the novel structure possesses a higher N-doping level than conventional graphene without the pierced structure. A much higher BET surface area was also achieved for the N-PGM than the conventional N-doped graphene microparticles (N-GM). Cyclic voltammetry indicated that the lithium-air battery with the N-PGM electrode has a better utilization for the graphene mass and a higher void volume for Li2O2 formation than that of the N-GM electrode. N-PGM also exhibits improved decomposition kinetics for Li oxide species yielded in the cathodic reaction. Charge and discharge measurements showed that the N-PGM lithium-air battery achieved an improved specific capacity and an enhanced cycle performance than when an N-GM electrode is used.

Disciplines

Engineering | Physical Sciences and Mathematics

Publication Details

Yuan, T., Zhang, W., Li, W., Song, C., He, Y., Razal, J. M., Ma, Z. & Chen, J. (2015). N-doped pierced graphene microparticles as a highly active electrocatalyst for Li-air batteries. 2D Materials, 2 (2), 024002-1 - 024002-7.

Authors

Tao Yuan, Weimin Zhang, Wen-Ting Li, Chuantao Song, Yu-Shi He, Joselito M. Razal, Zi-Feng Ma, and Jun Chen

N-doped pierced graphene microparticles as a highly active electrocatalyst for Li-air batteries

Tao Yuan[1, 3], Weimin Zhang[1, 3], Wen-Ting Li[1], Chuantao Song[1], Yu-Shi He[1], Joselito M Razal,[4] Zi-Feng Ma[1, 2, 5*], Jun Chen[3, 5*]

[1] Shanghai Electrochemical Energy Devices Research Center, School of Chemistry and Chemical Engineering, Shanghai Jiao Tong University, Shanghai 200240, China.

[3] Sinopoly Battery Research Centre, Shanghai 200241, China.

[2] ARC Centre of Excellence for Electromaterials Science, Intelligent Polymer Research Institute, Australian Institute of Innovative Materials, University of Wollongong, Wollongong, NSW 2500, Australia

[4] Institute for Frontier Materials, Deakin University, Geelong, VIC 3216, Australia

[5] Author to whom any correspondence should be addressed.

The first two authors contributed equally to this work.

Email: junc@uow.edu.au; zfma@sjtu.edu.cn

Abstract. In this work we report a novel scalable strategy to prepare 3D N-doped pierced graphene microparticles (N-PGM) with highly active performance as a lithium-air batterie electrode. This approach has combined the merits of both spray drying technology and hard template method. The pierced structured graphene microparticles were characterized physically and electrochemically. XPS and Raman spectra revealed that the novel structure possess a higher N-doping level than conventional graphene without the pierced structure. A much higher BET surface area was also achieved for the N-PGM than the conventional N-doped graphene microparticles (N-GM). Cyclic voltammetry indicated that the lithium-air battery with the N-PGM electrode has a better utilization for the graphene mass and a higher void volume for the Li_2O_2 formation than that of the N-GM electrode. N-PGM also exhibits improved decomposition kinetics for Li oxide species yielded in the cathodic reaction. Charge and discharge measurements showed that the N-PGM lithium air battery achieved an improved specific capacity and an enhanced cycle performance compared when N-GM electrode is used.

Keywords: Li-Air Battery, Graphene, Pierced Structure, Hard Template Method, N-doping

1. Introduction

Rechargeable lithium-air batteries have been receiving increasing attention as a sustainable energy technology because of their potential to offer 3 to 5 times the gravimetric energy density compared with conventional Li-ion batteries [1-3]. However, the real-world commercialization of such devices is still hindered by many issues from electrochemistry, chemistry and even technologies. These issues include

the low energy storage efficiency due to high electrochemical polarization corresponding to the charge/discharge voltage distance [4, 5], the poor reversibility especially at O_2 electrode side [6, 7], the poor stability of electrolytes which are easily decomposed at both sides [8-10], and the sensitivity to the contamination from the species such as H_2O and CO_2, [11-13] etc.

In order to increase the energy storage efficiency and reversibility for the electrochemical reactions within the batteries, much effort has been continuously devoted to explore highly active electrocatalysts and highly efficient electrodes with ideal structures to meet the requirements for achieving practical applications for Li air batteries. Typically, catalysts are metal oxides [14-19], metal nitrides [20, 21], doped carbon materials [22, 23], and precious metals [24, 25]. These electrocatalysts have all been developed based on the mechanistic hypothesis that they are able to facilitate good reversibility of oxygen reduction reactions (ORR) and oxygen evolution reactions (OER) with an electrochemical polarization as low as possible [18]. Among all the carbon materials, graphene has been particularly attracting interests due to its distinctive features such as high surface area, high electrical conductivity and thermal conductivity, excellent mechanical properties, and flexibility towards functionalization chemistries of functionalities [26-29].

In this paper, we combined the spray drying technology with hard template method in successfully preparing pierced textured graphene microparticles with high surface area. The as-made graphene microparticles have proved more highly efficient to be doped with N than the conventional porous graphene materials. Furthermore, the obtained N-doped graphene architectures were also fully characterized physically and electrochemically and showed promising results to be the potential active electrocatalysts for Li-air batteries.

2. Experimental

2.1. Synthesis of N-PGM

Graphene oxide was synthesized from natural graphite powder (Grade 230, Asbury Carbons) by a modified Hummer's method [30]. N-PGM were obtained according to the following procedure. Briefly, SiO_2 solid (particle size: ~15 nm, Aladdin) and GO suspension (1 mg mL^{-1}) were mixed together in an aqueous suspension with a mass ratio between SiO_2 and GO of 20:80. After ultrasonically dispersing for 1 hr, the aqueous mixture was loaded into a B-290 mini spray drier (Buchi, Swiss) under continuous stirring. The spray-dried product was further heated in a tube furnace under Ar/NH_3 (10 %) atmosphere with a heating rate of 10 ^oC min^{-1} to 1000 ^oC for 2 hrs with a flow rate of 50 ml min^{-1} to obtain N-doped graphene-encapsulated SiO_2 microparicles. The obtained microparticles were then dispersed in diluent HF solution for 1 hr to etch out SiO_2. The precipitate was collected by filtering and washed with deionized water and ethanol respectively until the filtrate became neutral. The sample was finally dried at 80 ^oC in a vacuum oven overnight. For comparison, N-GM without the hard template was also prepared by spray-drying method and the same calcination procedure.

2.2. Physical characterizations

The crystalline structure property of N-PGM was examined by X-ray diffraction (XRD) (Rigaku D/MAX-2200/PC). Raman spectra were obtained using a Bruker VERTEX 70. The morphology and microstructure of the spray-dried precursor and N-PGM were investigated using a FEI Nova SEM 230 ultra-high resolution Field Emission Scanning Electron Microscopy (FE-SEM) equipped (INCA X-Max 80, Oxford Instruments), and Transmission Election Microscopy (TEM) (JEM-2100F, JEOL Ltd., Japan). Porosity and Brunauer-Emmett-Teller (BET) surface areas of N-PGM were measured using a nitrogen sorption instrument (Micromeritics, ASAP2020). The surface properties of N-PGM were analyzed by X-ray photoelectron spectrometer (XPS, Kratos Axis Ultra DLD).

2.3. Electrochemical characterizations

The air electrode was prepared using the following procedure. The cathode slurry composed of N-PGM and polytetrafluoroethene (PTFE) in a weight ratio of 90:10 was obtained by uniformly dispersing the

materials in ethanol. A lithium metal anode, a glass fiber separator, an as-prepared air electrode and an electrolyte of 0.1 M LiTFSI (lithium bis-(trifluoromethanesulfonyl)-imide) in TEGDME (tetrathylene glycol dimethyl ether) were employed to assemble the Li-air battery in an argon-filled glove box. For comparison, the Li-air battery with N-GM electrode was also assembled following the same procedure as the above.

The electrochemical performance of the batteries was evaluated in a 1 atm O_2 atmosphere using a LAND CT2001A battery testing system at room temperature. Before the galvanostatic discharge/charge measurements, the batteries were placed in flowing pure oxygen for 1 hr and then transferred into the oxygen filled glass container for 6 hrs. The specific capacity and current density were calculated based on the loading amount of graphene material in the electrode.

3. Results and Discussion

Spray drying is an ideal approach of producing a dry powder from a liquid solution or suspension which is driven by a hot gas. Such a method typically leads to homogenous morphology for powder products in large scale [30]. The preparation of the three-dimensional pierced N-doped graphene has combined the advantages of both spray drying and hard template which are general, rapid, low-cost, scalable and effective. From the SEM and TEM images shown in Figure 1b and 1c, it can be seen that the SiO_2 nanoparticles were well mixed with graphene oxide after spray drying process which formed well dispersed microparticles. The as-made composites microparticles were calcined under Ar/NH_3 (10%) at high temperature to reduce GO into graphene and to introduce N into the graphene structure. The subsequent HF etching removes the SiO_2 in the microparticles and results in three dimensional pierced structure for the graphene microparticles. As shown in Figure 1a and 1d, both the spray-dried precursor and N-PGM product have both the precursor and N-PGM microparticles show irregular but well dispersed morphology and the average particle size is 2~3 μm.. And from Figure 1e and 1f, nanopores for the N-PGM are quite visible.

In order to investigate the crystalline properties of the N-PGM and N-GM and the spray-dried precursors, X-ray diffraction was performed and the results are shown in Figure 2. It is clear that the characteristic peak of GO at about 11° is visible in both the spray-dried precursors of N-PGM and the N-GM. Moreover, the spray-dried precursor of N-PGM show a broad peak centered at around $2\theta = 23°$, indicating low crystallinity of pore-forming agent of nano-SiO_2. For N-PGM and N-GM, the major diffraction peaks match with characteristic (002) peak of graphite at about 24°, which suggests that GO was efficiently reduced into graphene during the thermal treatment under Ar/NH_3 (10 %) atmosphere at 1000 °C for 2 hrs. The characteristic peak of SiO_2 is absent in the N-PGM sample, which can explain that most of the nano-SiO_2 hard template has been removed. Remarkably, the characteristic (002) peak of N-PGM is much wider than N-GM, which indicates low restacking of graphene sheets in N-PGM sample. In this way, nano-SiO_2 can help the dispersion of graphene sheets during the preparation process of N-PGM.

The porosity of the materials was studied by means of nitrogen sorption technique. The results are shown in Figure 3 and the specific values are summarized in Table 1. The hysteresis loop at high (P/P_0 = 0.85-1) pressure region in Figure 3a indicates large pores from mesopores to macropores are present in the N-PGM sample. While for N-GM sample (Figure 3b), the wider hysteresis loop from 0.45 to 1 of relative partial pressure (P/P_0) means mesoporous structure in the N-GM sample. Remarkably, the adsorbed quantity of N-PGM is almost an order of magnitude higher than N-GM, which depicts that the N-PGM has larger surface area and uniform pore structure. The BET surface areas of N-PGM and N-GM from the N_2 absorption measurement are 364.5 and 185.8 $m^2\ g^{-1}$, respectively. As shown in Figure 3a and 3b insets, N-PGM has an identical pore size distribution with hierarchically porous structure as its N-GM counterpart, but with higher average pore diameter and pore volume of ~21.5 nm and 2.0 $cm^3\ g^{-1}$ respectively (vs. 5.2 nm and 0.3 $cm^3\ g^{-1}$of N-GM sample, respectively).

The XPS spectra in Figure 4a revealed that the N-doping process occurred for both PGM and GM samples after annealing in Ar/NH_3 (10 %) atmosphere. It showed that the N-PGM and N-GM have ~2.5 at.% and ~1.9 at.% N, respectively. This information clearly indicated that the pierced structure of

graphene microparticles can obtain a higher N-doped level than the conventional structure. As shown in Figure 4b and 4c, the N1s peaks in the XPS spectra of N-PGM and N-GM samples were fitted into two peaks, which are pyridinic-N at a lower energy peak of 399.5 eV and quaternary-N at a higher energy peak of 400.6 eV[31]. The ratios of the pyridinic-N/quaternary-N for N-PGM and N-GM samples are calculated to be 1.59 and 2.94, respectively. The smaller ratio of the pyridinic-N/quaternary-N of N-PGM indicates more quaternary N (i.e. N that replaced the carbon atom in the graphene sheets and bonded to three carbon atoms) in carbon network of N-PGM. It is expected that better catalytic activity may be reflected in the N-PGM samples.

Raman spectra were recorded to characterize the N-PGM and N-GM which are shown in Figure 5. The peaks of D (~1355 cm^{-1}), G (~1600 cm^{-1}), 2D (~2700 cm^{-1}) and D' (~2930 cm^{-1}) were observed in the Raman spectra. The intensity ratio of D band and G band (I_D/I_G) offers useful information to evaluate the degree of crystallinity of graphene. In the present Raman spectra, the I_D/I_G intensity ratios of N-PGM and N-GM are calculated to be 1.03, and 0.97, respectively, which indicates that the obtained N-PGM and N-GM samples are predominantly hybridized in a sp^2 manner, thereby possessing good electronic conductivity. Besides, the value of I_D/I_G of N-PGM sample shows slight higher than that of N-GM, indicating more carbon atoms in the graphene sheets of the pierced structure have been replaced by nitrogen atoms, which is consistent with the results of XPS. [32].

The electrochemical catalytic activity of the electrodes toward ORR and OER has been investigated using cyclic voltammetry (CV) in an oxygen saturated 0.1 M LiTFSI/TEGDME electrolyte. As can be seen from Figure 6, both electrode show almost the same onset potential for ORR, which indicated that the pierced textured graphene does not have a different electrochemical kinetic compared with the conventional structure. The ORR for both electrodes peaked at about 2.4 V vs Li+/Li while the N-PGM electrode has the much higher current output than the N-GM electrode. This might be attributed the higher N-doping level and electrochemical active surface area of the pierced structures. Other factors that could contribute are the low re-stacking of graphene sheets, and the higher utilization of available graphene mass and void volume that facilitate the formation of Li_2O_2 [25]. In the anodic scan, the two peaks at 3.19 V and 3.44 V for the N-GM electrode can be respectively assigned to the first two OER pathways according to the elucidated decomposition mechanism below, while the third pathway occurs at the higher potential region without clear peak appeared in the CV curves [21]:

$$LiO_2 \rightarrow Li^+ + O_2 + e^- \quad (1)$$

$$Li_2O_2 \rightarrow 2Li^+ + O_2 + 2e^- \quad (2)$$

$$2Li_2O \rightarrow 4Li^+ + O_2 + 4e^- \quad (3)$$

In comparison, the two peaks are not distinguishable in the anodic scan for the N-PGM electrode and appear as one peak at 3.20. In addition, the negative shift of the total peaks area related to the OER for the N-PGM electrode compared with that for N-GM electrode obviously depicted the faster reaction kinetics due to the efficient diffusion pathway for O_2 product provide by the pierced structure.

The first discharge/discharge profiles of Li-O_2 batteries with the two different cathodes at between 2.0 V and 4.25 V are displayed in Figure 7. At the current density of 50 mA g^{-1}, the discharge voltage of the N-PGM cell is much higher while the charge voltage is lower than those of the cell with N-GM electrode. A specific discharge capacity of 14.3 Ah g^{-1} was obtained when using N-PGM as cathode which is much higher than 8.4 Ah g^{-1} for the N-GM cell. Such performance enhancement reveals that the lower electrochemical polarization and more reaction sites were obtained for the N-doped graphene after pierced texturing.

To evaluate the cycle performance of the Li-O_2 batteries, we carried out cycling tests using a current density of 200 mA g^{-1} with a fixed capacity of 1000 mAh g^{-1}. From Figure 8a, it can be seen that the distance between the charge and discharge voltage plateaus for the cell with N-PGM electrode showed a slight increase from 1.71 V to 1.84 V after 20 cycles. In comparison, the distance obtained by the cell with N-GM increased from 1.81 V to 2.09 V, which is much higher than that for N-PGM cell. The results suggest that the cell with N-PGM electrode has better cycle performance than when N-GM electrode is used. In addition, we can also observe at the first charge/discharge cycle that both cells show steady voltage plateaus. However, after five cycles, the charge voltage profiles for the N-GM cell kept

increasing while the discharge continuously decreased when the cycling approached the fix capacity of 1000 mAh g^{-1}. This is ascribed to the increase in electrochemical polarization of the N-GM cell. In contrast, the cell with N-PGM maintained steady voltage profiles within the same cycle range.

4. Conclusions

In conclusion, we developed an effective protocol to prepare pierced structured graphene using the combined spray drying technology and hard template method. The as-prepared graphene based composite was reduced and N-doped in NH_3/Ar at high temperature. The pierced structure was confirmed by SEM and TEM. XPS and Raman spectra proved that the pierced structure facilitates the N-doping process to achieve a high N-doping level. CV measurements showed that the N-PGM electrode exhibits similar ORR kinetic to the N-GM electrode with much higher graphene mass utilization, void volume for Li_2O_2 formation and faster decomposition kinetic in OER. A specific discharge capacity of 14.3 Ah g^{-1} was obtained when using N-PGM as cathode in comparison with 8.4 Ah g^{-1} for the N-GM lithium-air battery. The battery with N-PGM electrode has better cycle performance than that with N-GM electrode, which has been confirmed by cycling test. Such strategy can be used to produce N-PGM in large scale and could be realized in a continuous process, which suggests a promising potential for the commercial production of electrocatalysts for lithium air batteries.

Acknowledgement

Tao Yuan and Weimin Zhang contributed equally to this work. We are grateful for financial support for this work from the National Basic Research Program of China (2014CB239700, 2014CB932303), the Natural Science Foundation of China (21336003, 21403139), China Postdoctoral Science Foundation (2013M541510) and Australian Research Council (DP140100401, FT130100380). This work was also supported by Science and Technology Commission of Shanghai Municipality (14DZ2250800).

References

[1] Lu J, Li L, Park J-B, Sun Y-K, Wu F and Amine K 2014 *Chem. Rev.* **114** 5611-40

[2] Girishkumar G, McCloskey B, Luntz A C, Swanson S and Wilcke W 2010 *J. Phys. Chem. Lett.* **1** 2193-203

[3] Shao Y, Ding F, Xiao J, Zhang J, Xu W, Park S, Zhang J-G, Wang Y and Liu J 2013 *Adv. Funct. Mater.* **23** 987-1004

[4] Zhang S S, Foster D and Read J 2010 *J. Power Sources* **195** 1235-40

[5] Freunberger S A, Chen Y, Peng Z, Griffin J M, Hardwick L J, Bardé F, Novák P and Bruce P G 2011 *J. Am. Chem. Soc.* **133** 8040-7

[6] McCloskey B D, Speidel A, Scheffler R, Miller D C, Viswanathan V, Hummelshøj J S, Nørskov J K and Luntz A C 2012 *J. Phys. Chem. Lett.* **3** 997-1001

[7] Xu W, Viswanathan V V, Wang D, Towne S A, Xiao J, Nie Z, Hu D and Zhang J-G 2011 *J. Power Sources* **196** 3894-9

[8] Elia G A, Hassoun J, Kwak W J, Sun Y K, Scrosati B, Mueller F, Bresser D, Passerini S, Oberhumer P, Tsiouvaras N and Reiter J 2014 *Nano Lett.* **14** 6572-7

[9] Mozhzhukhina N, Méndez De Leo L P and Calvo E J 2013 *J. Phys. Chem. C* **117** 18375-80

[10] Zhang Z, Lu J, Assary R S, Du P, Wang H-H, Sun Y-K, Qin Y, Lau K C, Greeley J, Redfern P C, Iddir H, Curtiss L A and Amine K 2011 *J. Phys. Chem. C* **115** 25535-42

[11] Lim H-K, Lim H-D, Park K-Y, Seo D-H, Gwon H, Hong J, Goddard W A, Kim H and Kang K 2013 *J. Am. Chem. Soc.* **135** 9733-42

[12] Gowda S R, Brunet A, Wallraff G M and McCloskey B D 2012 *J. Phys. Chem. Lett.* **4** 276-9

[13] Zhang T and Zhou H 2013 *Nat Commun* **4** 1817

[14] Wu D, Zhang F, Liang H and Feng X 2012 *Chem. Soc. Rev.* **41** 6160-77

[15] Zhao G, Xu Z and Sun K 2013 *J. Mater. Chem. A* **1** 12862-7

[16] Zhao G, Niu Y, Zhang L and Sun K 2014 *J. Power Sources* **270** 386-90

[17] Wang J, Jin H, He Y, Lin D, Liu A, Wang S and Wang J 2014 *Nanoscale* **6** 7204-8
[18] Ryu W-H, Yoon T-H, Song S H, Jeon S, Park Y-J and Kim I-D 2013 *Nano Lett.* **13** 4190-7
[19] Li Y, Guo K, Li J, Dong X, Yuan T, Li X and Yang H 2014 *ACS Appl. Mater. Interfaces* DOI: 10.1021/am505718k
[20] Shui J-L, Karan N K, Balasubramanian M, Li S-Y and Liu D-J 2012 *J. Am. Chem. Soc.* **134** 16654-61
[21] Li F, Ohnishi R, Yamada Y, Kubota J, Domen K, Yamada A and Zhou H 2013 *Chem. Commun.* **49** 1175-7
[22] Shui J, Du F, Xue C, Li Q and Dai L 2014 *ACS Nano* **8** 3015-22
[23] Li L and Manthiram A 2014 *Adv. Energy Mater.* **4** DOI: 10.1002/aenm.201301795
[24] Dong S, Chen X, Wang S, Gu L, Zhang L, Wang X, Zhou X, Liu Z, Han P, Duan Y, Xu H, Yao J, Zhang C, Zhang K, Cui G and Chen L 2012 *ChemSusChem* **5** 1712-5
[25] Li J, Zhao Y, Zou M, Wu C, Huang Z and Guan L 2014 *ACS Appl. Mater. Interfaces* **6** 12479-85
[26] Allen M J, Tung V C and Kaner R B 2009 *Chem. Rev.* **110** 132-45
[27] Ambrosi A, Chua C K, Bonanni A and Pumera M 2014 *Chem. Rev.* **114** 7150-88
[28] Chen D, Feng H and Li J 2012 *Chem. Rev.* **112** 6027-53
[29] Chua C K and Pumera M 2013 *Chem. Soc. Rev.* **42** 3222-33
[30] Yuan T, Li W-T, Zhang W, He Y-S, Zhang C, Liao X-Z and Ma Z-F 2014 *Ind. Eng. Chem. Res.* **53** 10849-57
[31] Li X, Wang H, Robinson J T, Sanchez H, Diankov G and Dai H 2009 *J. Am. Chem. Soc.* **131** 15939-44
[32] Ferrari A and Robertson J 2000 *Phys. Rev. B* **61** 14095-107

Table 1 BET surface area, pore volume, and average pore width for N-PGM and N-GM calculated from Figure 3.

Samples	BET Surface Area (m^2 g^{-1})	Pore Volume (cm^3 g^{-1})	Average pore width (nm)
N-PGM	364.5	2.0	21.5
N-GM	185.8	0.3	5.2

Figure Captions

Figure 1 SEM (a, b, d, e) and TEM (c, f) images of spray-dried nano-SiO_2/graphene oxide composite before (a, b, c) and after the removal of SiO_2 hard template (d, e, f).

Figure 2 XRD patterns of spray-dried precursors for both N-PGM and N-GM and the corresponding materials after calcination.

Figure 3 Nitrogen adsorption-desorption isotherm and BJH pore size distribution plots (insets) of (a) N-PGM and (b) N-GM.

Figure 4 XPS survey spectrum of the N-PGM and N-GM samples (a) and High-resolution XPS spectra of N1s for N-PGM (b) and N-GM samples (c).

Figure 5 Raman spectra of N-PGM and N-GM.

Figure 6 CV curves of N-PGM and N-GM electrodes in the oxygen saturated 0.1 M LiTFSI/TEGDME electrolyte at a scanning rate of 0.5 mV s^{-1}.

Figure 7 The first discharge/charge curves of Li-O_2 batteries using N-PGM and N-GM as cathodic materials respectively at a low current density of 50 mA g^{-1} within the voltage window between 2.0 and 4.2 V.

Figure 8 Voltage profiles of Li-O_2 battery using (a) N-PGM and (b) N-GM as cathodic materials at a current density of 200 mA g^{-1} with a fixed capacity of 1000 mAh g^{-1} at various cycles.

Figure 1

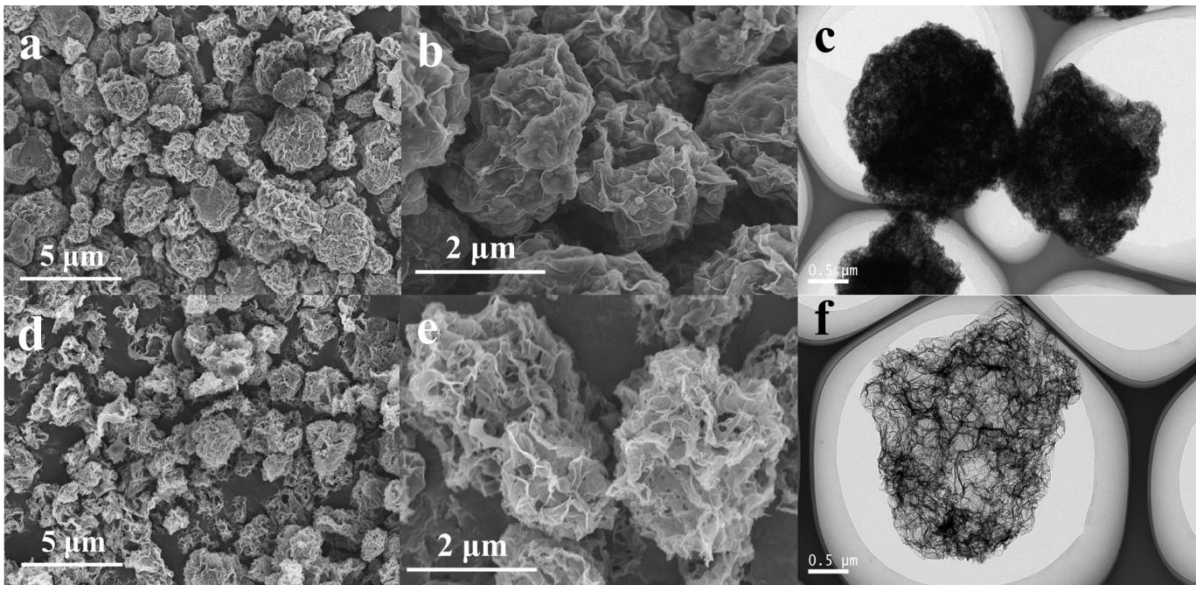

Figure 2

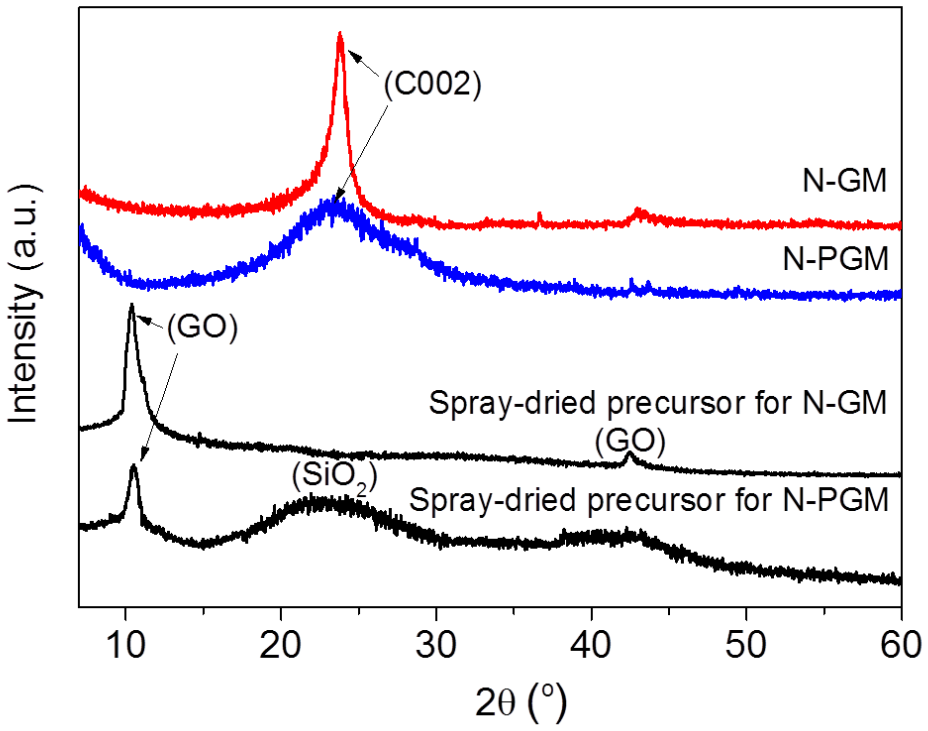
(C002)
N-GM
N-PGM
(GO)
Spray-dried precursor for N-GM
(GO)
(SiO2)
Spray-dried precursor for N-PGM
Intensity (a.u.)
10
20
30
40
50
60
2θ (°)

Figure 3

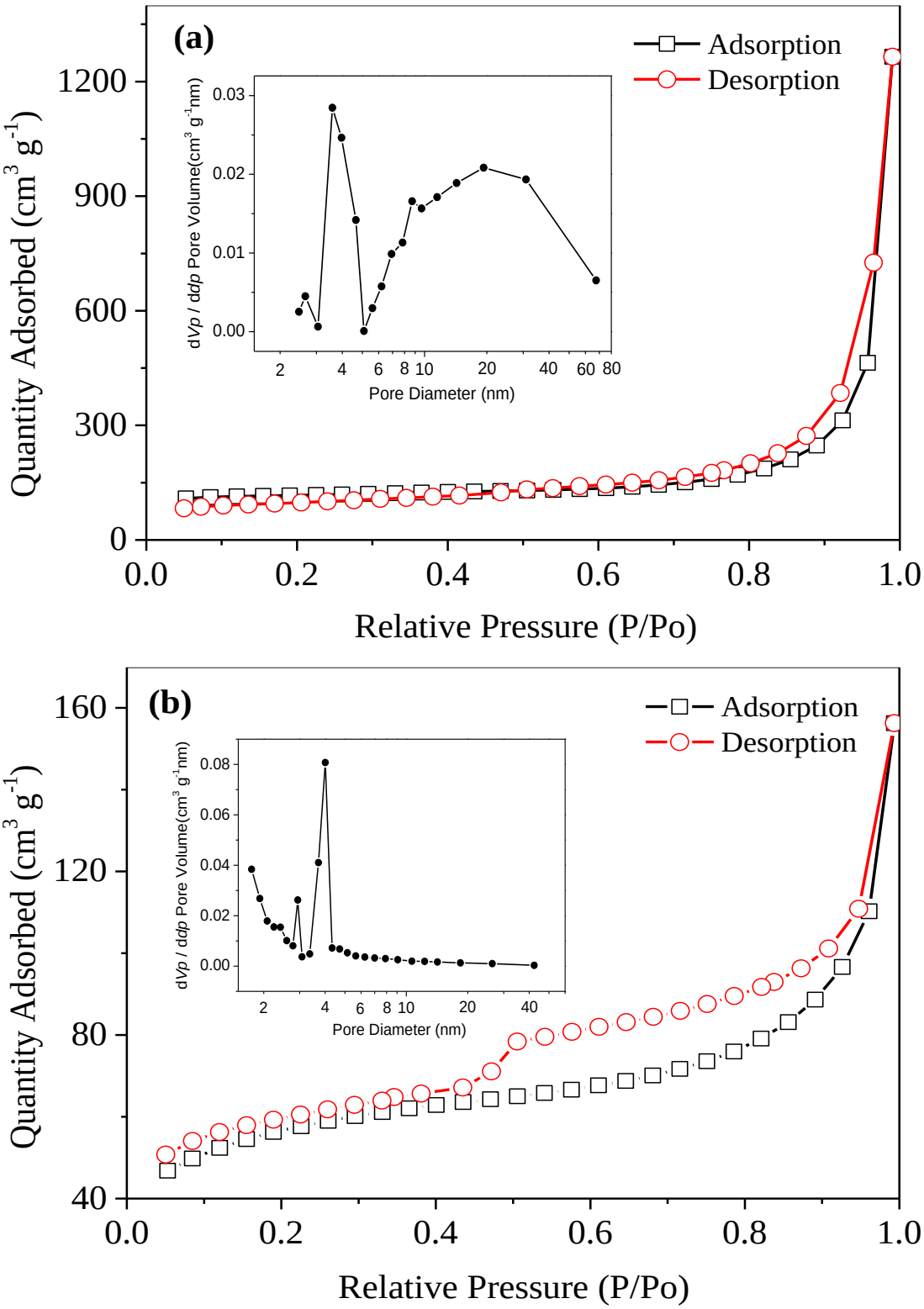
(a)
Adsorption
Desorption
Quantity Adsorbed (cm3 g-1)
Relative Pressure (P/Po)
dVp / ddp Pore Volume(cm3 g-1nm)
Pore Diameter (nm)
(b)
Adsorption
Desorption
Quantity Adsorbed (cm3 g-1)
Relative Pressure (P/Po)
dVp / ddp Pore Volume(cm3 g-1nm)
Pore Diameter (nm)

Figure 4

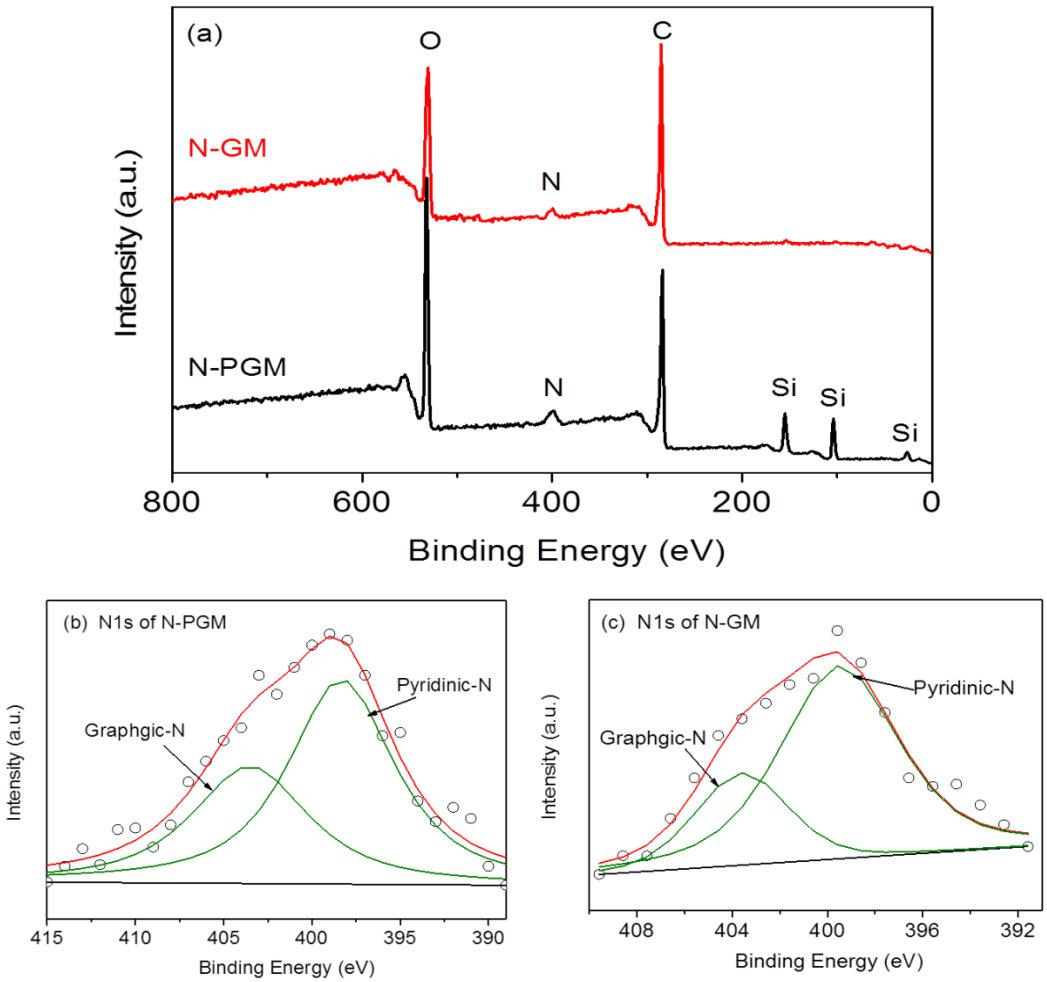
(a)
O
C
N-GM
N
N-PGM
N
Si
Si
Si
Intensity (a.u.)
800
600
400
200
0
Binding Energy (eV)
(b) N1s of N-PGM
Pyridinic-N
Graphgic-N
Intensity (a.u.)
415
410
405
400
395
390
Binding Energy (eV)
(c) N1s of N-GM
Pyridinic-N
Graphgic-N
Intensity (a.u.)
408
404
400
396
392
Binding Energy (eV)

Figure 5

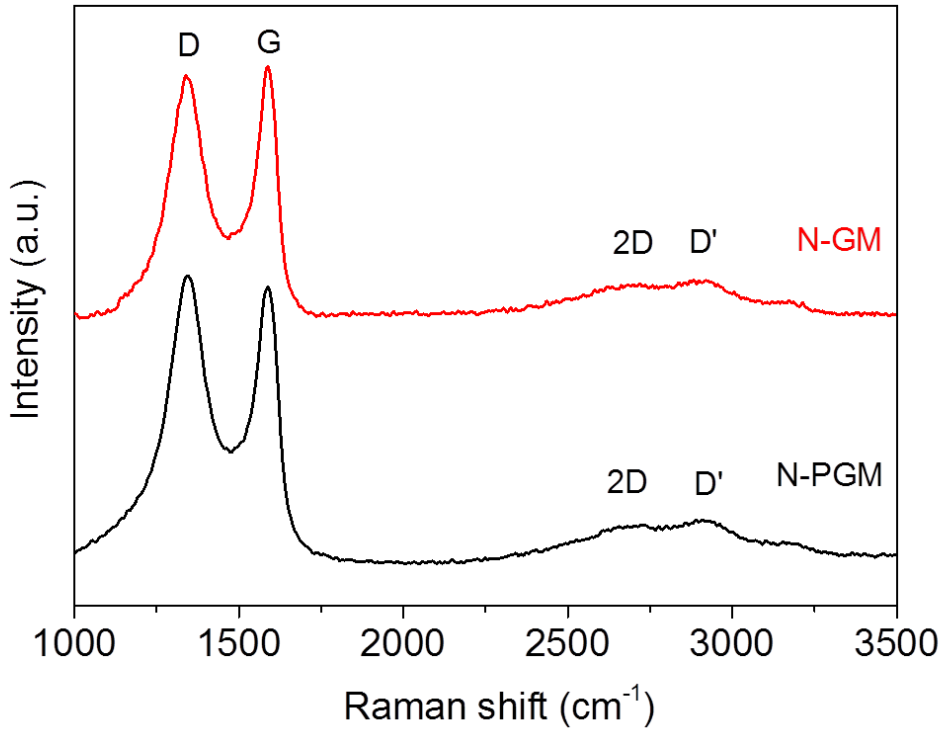
D
G
2D
D'
N-GM
2D
D'
N-PGM
Intensity (a.u.)
1000
1500
2000
2500
3000
3500
Raman shift (cm-1)

Figure 6

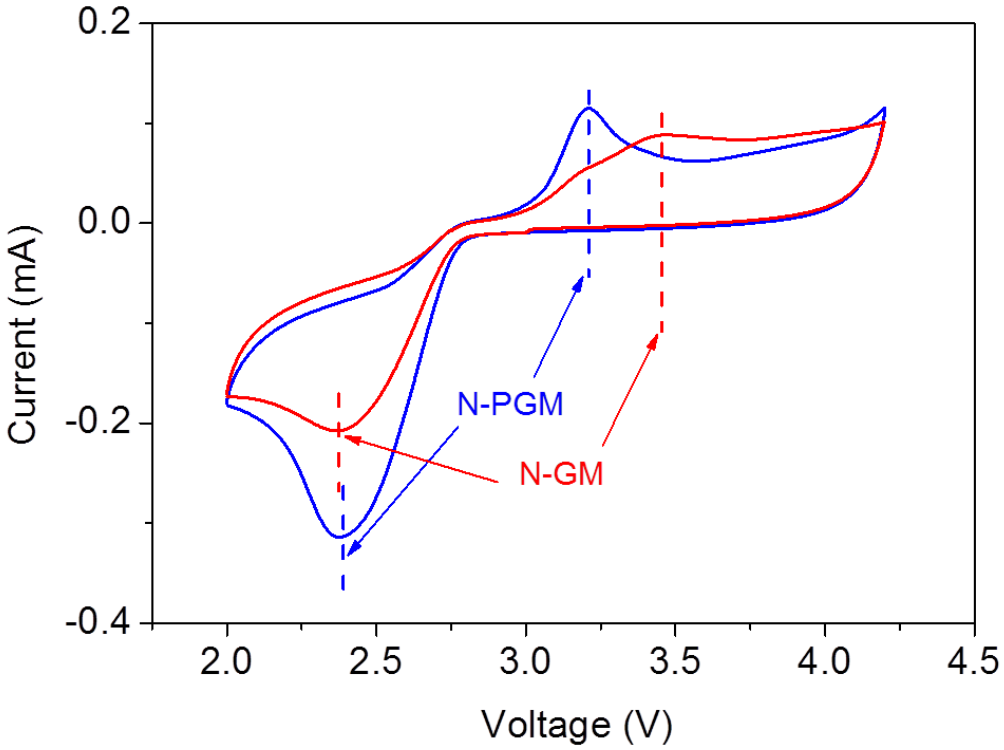

Figure 7

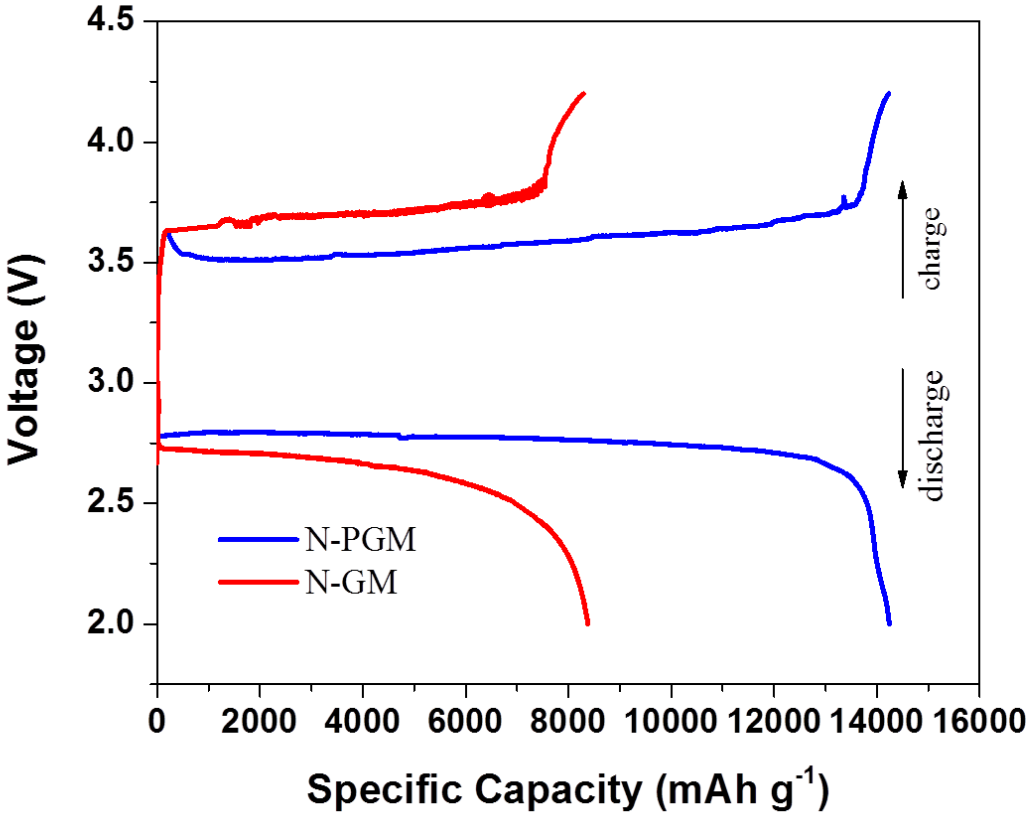
4.5
4.0
3.5
3.0
2.5
2.0
Voltage (V)
0
2000
4000
6000
8000
10000
12000
14000
16000
Specific Capacity (mAh g-1)
charge
discharge
N-PGM
N-GM

Figure 8

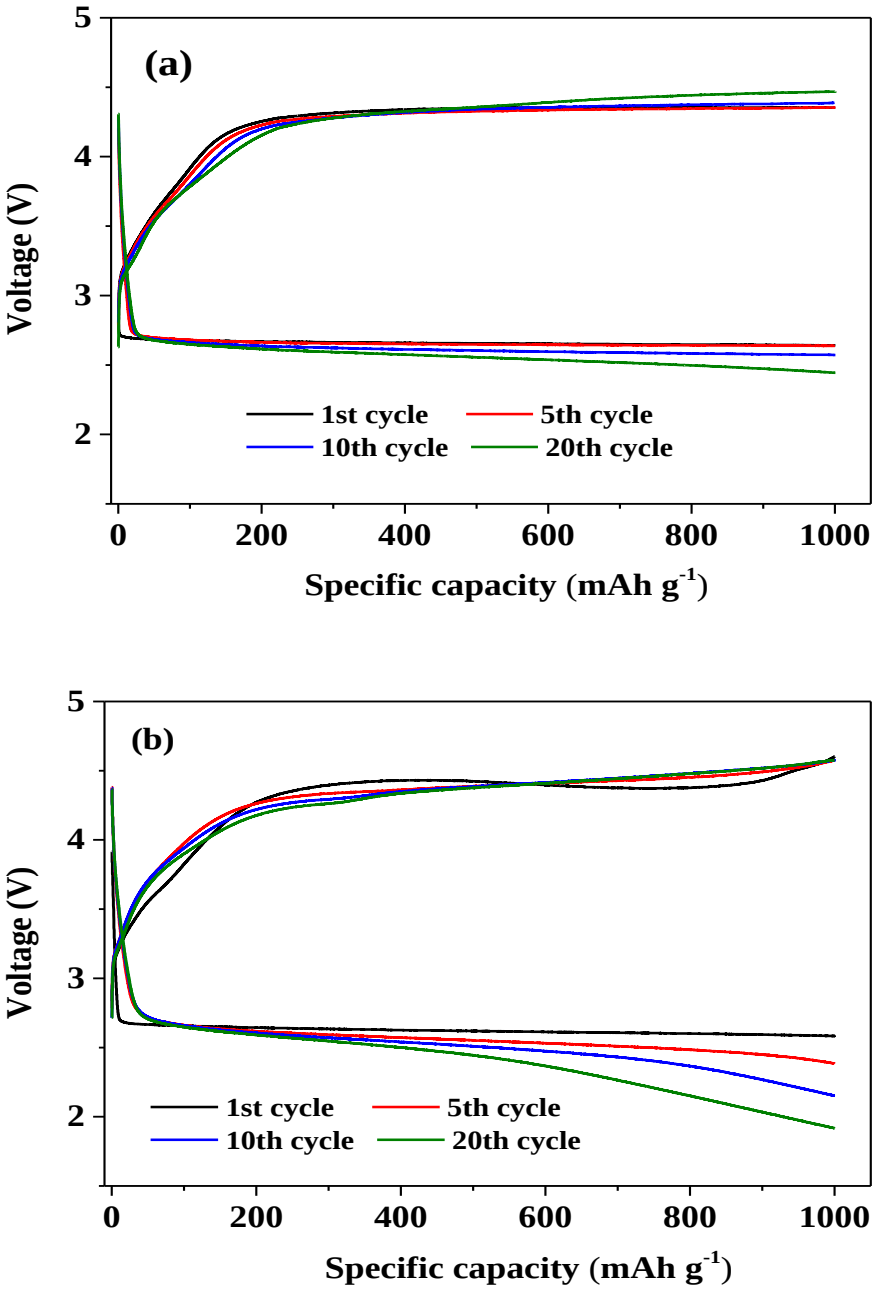
(a)
Voltage (V)
Specific capacity (mAh g-1)
1st cycle
5th cycle
10th cycle
20th cycle
(b)
Voltage (V)
Specific capacity (mAh g-1)
1st cycle
5th cycle
10th cycle
20th cycle